8916–8929 *Nucleic Acids Research, 2017, Vol. 45, No. 15* *Published online 10 July 2017*
doi: 10.1093/nar/gkx596

A novel nucleoid-associated protein coordinates chromosome replication and chromosome partition

James A. Taylor[1], Gaël Panis[2], Patrick H. Viollier[2] and Gregory T. Marczynski[1,*]

[1]Department of Microbiology and Immunology, McGill University, 3775 University St., Montreal, QC H3A 2B4, Canada and [2]Department of Microbiology and Molecular Medicine, University of Geneva Medical School, 1 rue Michel-Servet, CH-1211 Geneva 4, Switzerland

Received March 21, 2017; Revised June 16, 2017; Editorial Decision June 16, 2017; Accepted July 05, 2017

ABSTRACT

We searched for regulators of chromosome replication in the cell cycle model *Caulobacter crescentus* and found a novel DNA-binding protein (GapR) that selectively aids the initiation of chromosome replication and the initial steps of chromosome partitioning. The protein binds the chromosome origin of replication (*Cori*) and has higher-affinity binding to mutated *Cori*-DNA that increases *Cori*-plasmid replication *in vivo*. *gapR* gene expression is essential for normal rapid growth and sufficient GapR levels are required for the correct timing of chromosome replication. Whole genome ChIP-seq identified dynamic DNA-binding distributions for GapR, with the strongest associations at the partitioning (*parABS*) locus near *Cori*. Using molecular-genetic and fluorescence microscopy experiments, we showed that GapR also promotes the first steps of chromosome partitioning, the initial separation of the duplicated *parS* loci following replication from *Cori*. This separation occurs before the *parABS*-dependent partitioning phase. Therefore, this early separation, whose mechanisms is not known, coincides with the poorly defined mechanism(s) that establishes chromosome asymmetry: *C. crescentus* chromosomes are partitioned to distinct cell-poles which develop into replicating and non-replicating cell-types. We propose that GapR coordinates chromosome replication with asymmetry-establishing chromosome separation, noting that both roles are consistent with the phylogenetic restriction of *GapR* to asymmetrically dividing bacteria.

INTRODUCTION

Faithful genome duplication requires dedicated mechanisms to coordinate cell cycle events but for bacteria such coordination is especially problematic. For example, bacteria evolved cell cycle programs where chromosome replication and chromosome partitioning overlap (1). Once started, the cell is committed to chromosome replication that lasts most of the cell division cycle. Replication timing is critical since delays also reduce competitive fitness while commitment in unfavorable conditions risks genome damage and cell death (2). Since bacterial chromosomes use only one origin of replication, the bacterial strategy for regulating chromosome replication implies that much information is processed through this unique origin and this further implies complex protein-binding interactions (3,4). Our working hypothesis is that novel DNA-binding proteins evolved to coordinate chromosome replication and partitioning.

Caulobacter crescentus provides an excellent model to study the bacterial cell cycle (5). Its dimorphic growth presents distinct programs of chromosome replication and chromosome partitioning that are being exploited for detailed analysis. *C. crescentus* swarmer (*Sw*) cells present the motile and non-replicating cell stage. As the cell cycle proceeds, the *Sw* cells differentiate into stalked (*St*) cells that present the non-motile but replicating stage. Therefore, the initiation of chromosome replication is coordinated with the cell differentiation from the *Sw* to the *St* cell stages. Next, *C. crescentus* cell division proceeds asymmetrically as the elongating cell builds a new flagellum at the new *Sw* pole opposite the old *St* cell pole. Chromosome partitioning starts very soon after the initiation of chromosome replication and both cell cycle processes overlap the elaboration of asymmetric cell division that ultimately yields a *Sw* cell and a *St* cell (6). Therefore, this cell division program produces distinct cells, each with distinct non-replicating (*Sw*) and replicating (*St*) chromosomes.

We study the *C. crescentus* chromosome origin of replication (*Cori*; Figure 1A) and our experiments address how *Cori* directs the non-replicating *Sw* and the replicating *St* chromosome states. In this report, we identify a novel DNA-binding protein (GapR) and show that GapR is a dynamic-binding nucleoid-associated protein that selectively facilitates the initiation of chromosome replication and the ear-

*To whom correspondence should be addressed. Tel: +1 514 398 3917; Fax: +1 514 398 7052; Email: gregory.marczynski@mcgill.ca
Present address: James A. Taylor, Department of Cellular and Molecular Medicine, University of Ottawa, 451 Smyth Road, Ottawa, ON K1H 8L1, Canada.

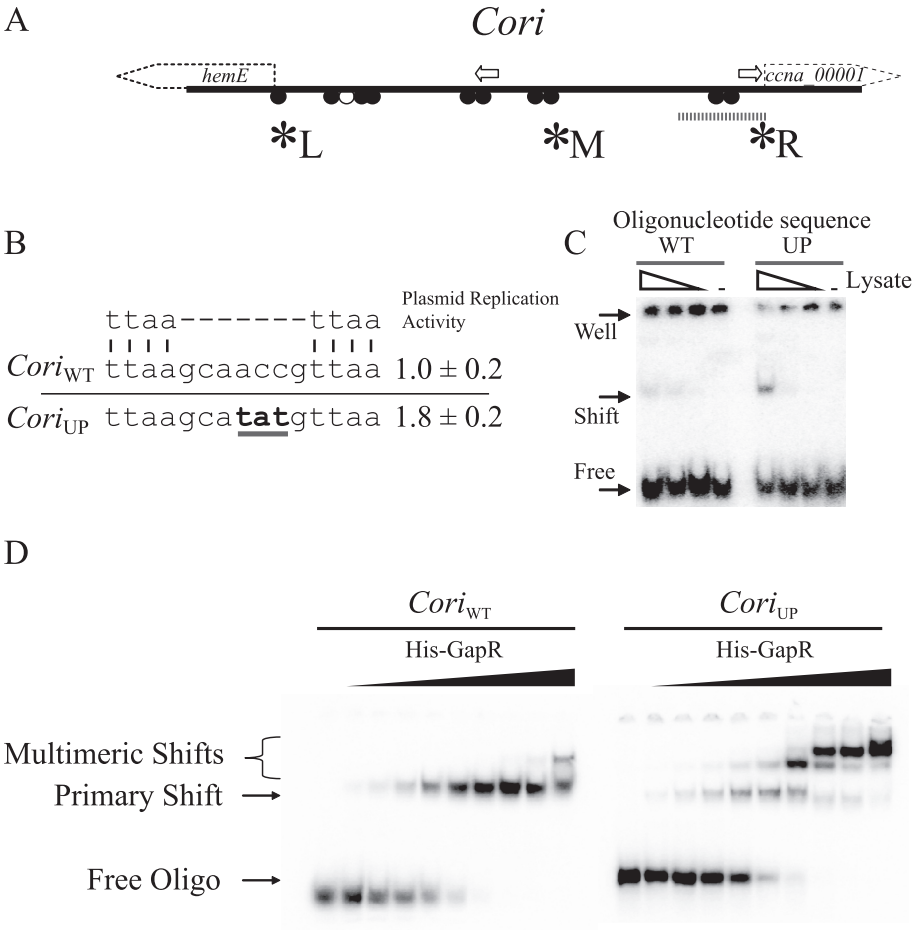

Figure 1. Identification of GapR (CCNA_03428) as a factor promoting chromosome replication. (**A**) A schematic of *Cori* including CtrA binding sites (black circles indicate half-sites), strong DnaA binding sites (two open arrows) and the most conserved region, studied in Taylor *et al.* (7) (underline). Flanking coding sequences (*hemE* and *ccna_00001*) are shown. The positions of three probes used for qChIP analysis in Figure 3B are marked by asterisks together with their identifying letters, for *Cori* L, *Cori* M and *Cori* R. (**B**) The ability of WT and mutant *Cori* DNA to drive autonomous plasmid replication was assessed by enzyme activity from the *gusA* gene reporting plasmid copy number. The higher $Cori_{UP}$ replication was assessed from five independent assays. The alignment shows WT sequence compared to up-replication mutant sequence ($Cori_{UP}$; mutation underlined) together with the plasmid copy number (relative to WT). The position of a consensus CtrA binding site is indicated above the alignment. (**C**) EMSA experiments showing that a factor present in a cleared *C. crescentus* cell lysate binds more strongly to oligonucleotides carrying sequences from $Cori_{UP}$ than from $Cori_{WT}$. 40 bp annealed oligonucleotides carrying either the $Cori_{WT}$ or $Cori_{UP}$ sequences were incubated with ten-fold dilutions of partially fractionated cleared cell lysate (left to right, dilutions indicated by a wedge) or in buffer alone (lanes marked '-') and run on a non-denaturing gel. A greater fraction of the $Cori_{UP}$ oligonucleotides are shifted by the same lysate concentrations than the $Cori_{WT}$ oligonucleotides. (**D**) EMSA experiments comparing how equal concentrations of His-GapR protein (purified from *E. coli*) bind to the same annealed oligonucleotides as in (C). For each gel, in the leftmost lane oligonucleotides were incubated in buffer alone. Reactions in the right-hand lane were incubated with 500 nM His-GapR, and lanes to the left of this contained a two-fold dilution series of His-GapR. Preferential protein binding to the $Cori_{UP}$ oligonucleotide was replicated 4 time.

liest stage of chromosome partitioning. We propose that GapR connects the start of two overlapping yet otherwise mechanistically different cell cycle processes that ultimately create two functionally district chromosomes in an asymmetrically dividing cell.

MATERIALS AND METHODS

Bacterial strains and plasmids

Caulobacter crescentus strains and plasmids used in this study are described in Supplementary Tables S3 and S4, respectively. Construction of new plasmids and *C. crescentus* strains is described in the supplementary material. *Escherichia coli* strains were grown in LB media supplemented with ampicillin (100 μg/ml) or kanamycin (50 μg/ml) where noted. *Caulobacter crescentus* strains were grown in PYE or M2G media as noted, with xylose (0.5% w/v), glucose (0.2% w/v), ampicillin (20 μg/ml), chloramphenicol (1 μg/ml), spectinomycin (100 μg/ml) and streptomycin (2.5 μg/ml) added as described.

Cell fractionation and protein purification

The initial cell fractionation carried out to purify GapR from whole cell lysates as well as the purification buffer compositions are described in Supplementary Figure S1. Recombinant His-GapR and GST-CtrA were purified as described in supplementary methods.

EMSA reactions

EMSA reactions were performed with radio-labeled oligonucleotides as previously described (7) but in EMSA buffer consisting of 20 mM Tris–HCl pH 8, 100 mM KCl, 5 mM $MgCl_2$, 1 mM $CaCl_2$, 2 mM DTT, 50 μg ml^{-1} BSA. Briefly, radio-labeled annealed oligonucleotides were incubated with various protein fractions in the EMSA buffer on ice for 30 min before being loaded directly onto a 8% polyacrylamide gel in 1× TBE. The sequences of the oligonucleotides used for $Cori_{WT}$ and $Cori_{UP}$ are listed in Supplementary Table S5 ('WT' and 'UP' pairs respectively).

Autonomous replication assay

Autonomous replication assays were performed as previously described (7). Briefly, plasmids carrying the reporter gene *gusA* and relying on *Cori* or $Cori_{UP}$ for their replication were transformed by electroporation into GM1609 or derivatives, and cells were plated onto selective media (PYE + ampicillin). GM1609 can be selected for beta-lactamase resistance plasmids, because it has a deletion in its natural beta-lactamase gene. GM1609 is otherwise identical to the standard wild type strain NA1000. After four days, colonies were washed off into PYE media, and assayed for GusA activity to report plasmid copy number.

Immunoblotting

Antibodies were raised in rabbits against GapR (at the McGill Animal Facility) and CtrA (at MediMabs, Montreal), or have previously been described (7). All were used in immunoblotting at a 1:10,000 dilution. Secondary anti-rabbit antibodies conjugated to horse radish peroxidase (Sigma) were also used at a 1:10 000 dilution. Immunoblots from SDS-PAGE onto PVDF membrane were visualized using 'Western Lightning' reagents (Perkin-Elmer) and a VersaDoc system (BioRad).

Chromatin ImmunoPrecipitation coupled to deep sequencing (ChIP-Seq)

ChIP-seq was carried out essentially as previously described (8) using mid-log phase cells ($O.D._{660\,nm} \sim 0.5$), cultured in PYE or with an extra 10 min treatment with antibiotics (Rifampicin 30 μg/ml; Novobiocin 100 μg/ml, chloramphenicol 1 μg/ml). To form the immuno-complexes, the precleared supernatants were incubated overnight at 4°C with GapR Polyclonal antibodies (1:1000 dilution). HiSeq 2000 runs of barcoded ChIP-Seq libraries yielded several million reads that were mapped to the *Caulobacter crescentus* NA1000 (NC_011916, circular form) and analyzed as described in supplementary methods. Briefly, the genome was subdivided into 1 bp (isolated regions) or 50 bp (full chromosome) probes, and we calculated the percentage of reads per probe as a function of the total number of reads. Analyzed data illustrated in Figure 3A using the Circos Software (9) are provided in Dataset S1 (50 bp resolution). Figure 3C focuses on the *par* and the *Cori* regions (4 026 155 to 1150 bp on the circular *Caulobacter crescentus* genome), analyzed datasets are provided in Dataset S2 (full chromosome at 50 bp resolution) and Dataset S3 (*par*ABS and *Cori* regions at 1 bp resolution). Sequence data have been deposited to the Gene Expression Omnibus (GEO) database (GSE95535 series, accession nos. GSM2516003–GSM2516008).

Quantitative chromatin immunoprecipitation (qChIP)

Chromatin immunoprecipitation was performed as previously described but using 1:1000 anti-GapR (8). For mixed culture experiments, log phase cultures in PYE were treated with antibiotics (where described) for 10 min. qPCR was performed with oligonucleotide primers described in Supplementary Table S5 (primer pairs listed as 'q[gene name] fwd/rev') using the FastStart Universal SYBR green qPCR kit (Roche) on a Rotorgene 6000 thermocycler (Corbett) or a CFX 96 thermocycler (Bio-Rad) and analyzed using the Rotorgene (Corbett) or CFX Manager (Bio-Rad) software package. All qPCR reactions were validated by standard curves using template serial dilutions. Amplification efficiencies calculated from the slopes of these curves lay between 95% and 105%, with the R^2 values for each curve being >0.98.

Flow cytometry to measure the fraction of cells that started chromosome replication

Flow cytometry was performed on synchronous cultures that had been isolated with a Percoll density gradient (10) using an replication run-out protocol that allowed cells to finish any rounds of chromosome replication that had already initiated, as previously described (2). Briefly, freshly isolated swarmer cells were transferred to PYE containing glucose or xylose and samples were taken from the synchronized culture at various times and transferred into media containing 60 μg/ml rifampicin and 35 μg/ml cephalexin for at least three hours. Ethanol was then added to 70% final concentration to fix cells, and samples washed once with 70% ethanol and were stored at 4°C prior to analysis. Staining and analysis were performed as described (2).

Microscopy

Fluorescence and DIC images were captured using a Zeiss Axiovert200M with a 100× objective at the McGill University Life Sciences Complex Advanced BioImaging Facility. For fluorescence microscopy experiments, samples were imaged on 1% agarose pads in water or PYE media for live cell time-lapse studies. For all experiments comparing GFP-ParB localization in synchronized cells, we also took control flow cytometry samples (see above) concurrently with their microscopic imaging to confirm that the fraction of cells that started chromosome replication were comparable between matched strains. This control distinguished replication timing defects from chromosome partitioning (GFP-ParB motion) defects in Figures 5 and 6. GFP-ParB localization was scored by inspecting images with large cell numbers (n-values are given in the respective figure legends).

RESULTS

Discovery of a novel DNA-binding protein

As part of our search for new regulators of the *C. crescentus* origin of chromosome replication (*Cori*) we previously reported a 5 bp mutation within the most conserved region of *Cori* (Figure 1A) that causes a ∼2 fold increase in *Cori* autonomous replication (7). Here, we introduced a 3 bp mutation into a similar position in *Cori* and observed that this mutation also caused a ∼2-fold increase in *Cori* replication (Figure 1B). We hypothesized that this mutation ($Cori_{UP}$) altered the binding of a protein to *Cori*, and we sought to identify it by an electrophoretic mobility shift assay (EMSA). We probed *C. crescentus* cell lysates using radio-labeled annealed oligonucleotides carrying either the natural *Cori* sequence ($Cori_{WT}$) or the mutated up-replication sequence ($Cori_{UP}$). We found that the $Cori_{UP}$ sequence had a higher affinity for an unknown protein present in the cell lysate (Figure 1C). We purified this protein by biochemical fractionation (see Supplementary Figure S1 and methods) and identified it using liquid chromatography/tandem mass-spectrometry as the product of the *ccna_03428* gene, previously annotated as a hypothetical cytosolic protein (11), that is highly conserved in alphaproteobacteria, which was named *GapR*. We PCR cloned and purified N-terminally poly-histidine tagged GapR from *E. coli* and confirmed that this protein preparation also differentially shifts the $Cori_{WT}$ and $Cori_{UP}$ oligonucleotides (Figure 1D).

GapR is essential for normal rapid growth

We attempted to delete the *GapR* coding sequence and to replace it with the omega antibiotic resistance cassette through two-step homologous recombination. However, we could only delete *GapR* when we supplied an extra *GapR* gene on a replicating plasmid (see Supplementary Table S1). A high-throughput transposon mutagenesis screen also proposed that *GapR* is essential in *C. crescentus* (11). To study how removing *GapR* might affect *C. crescentus*, we replaced the plasmid covering the deletion with a plasmid carrying *GapR* under the control of a xylose inducible promoter (pJT157; see Supplementary Figure S2A). This strain (GM3817) now required xylose for growth and died when shifted to glucose (Supplementary Figure S2B). Interestingly, while most cells die during prolonged depletion of GapR, a few cells survive. These derived '*ΔGapR* suppressor strains' can grow indefinitely without GapR and resemble wild type (WT) cells with key defects (described further below and in supplementary data). While these experiments were done under rapid growth conditions in rich (PYE) media, we also observed that these same GM3817 cells died under slow growth conditions in minimal (M2G/glucose) media. The derived *ΔGapR* suppressor strains grew slower than WT and their growth was stimulated by genetically restoring *gapR* on plasmid pJT165 (supplementary data). Therefore, GapR is essential for rapid growth and this requirement suggests that GapR regulates or optimizes essential cell cycle functions.

GapR is required for timing chromosome replication

Our analysis indicated that GapR positively promotes replication by directly binding to *Cori* (Figure 1), and therefore we next tested replication initiation in conditionally expressing *Pxyl::GapR* GM3817 cells. Chromosome replication initiates from *Cori* when swarmer (*Sw*) cells differentiate into stalked (*St*) cells. Therefore, synchronous *C. crescentus Sw* cell cultures of WT parental GM1609 and GM3817 were isolated (10) and placed in media supplemented with xylose or glucose. Samples of the synchronized cultures were removed at 0, 30, 60 and 90 minutes post-synchronization and treated with antibiotics to prevent new rounds of chromosome replication and cell division. Since this treatment allows ongoing chromosome replication to finish, this method distinguishes replicating and non-replicating cells. Cells that initiated chromosome replication when sampled will complete replication (but not cell division), and will have two complete chromosomes and cells which have not initiated replication will retain only one chromosome (see Figure 2A).

As expected, cells from WT GM1609 differentiated rapidly and initiated chromosome replication by 30 min and GM1609 showed no replication timing differences between xylose or glucose media (Figure 2B). In contrast, even with xylose to induce GapR, GM3817 cells displayed a pronounced delay in replication initiation, and most of these cells failed to initiate replication in glucose media without xylose to induce GapR expression (Figure 2C). Immunoblots show that GapR levels in GM3817 grown in xylose were ∼10% of the WT cells (not shown). Therefore, both replication delays (WT versus GM3817 Figure 2BC and xylose versus glucose Figure 2C) are attributable to lower GapR levels.

We also assayed the synchronized cells in Figure 2 by tracking the abundance of two marker proteins that are degraded at the *Sw* to *St* cell transition. Immunoblot analysis demonstrated that both the master cell cycle regulator CtrA (Figure 2D) and the chemotaxis protein McpA (Supplementary Figure S3) were degraded at the appropriate cell cycle times. For example, CtrA was completely degraded in all cultures by 30 min when all WT GM1609 cells had initiated chromosome replication. Interestingly, both marker proteins show a delayed return late in the cell cycle of the GM3817 cells suggesting that later stalked cell programs (e.g. cell division) are delayed with reduced GapR levels. In summary, while GapR probably aids later cell cycle progression, it does not significantly influence the earlier *Sw* to *St* cell differentiation and yet lower GapR levels selectively retard the timely start of chromosome replication, implying the selective activity at *Cori*.

Direct GapR binding to *Cori* promotes chromosome replication *in vivo*

If GapR is promoting chromosome replication by directly binding to *Cori*, then increasing *Cori* affinity for GapR should ameliorate the delayed replication seen above during GapR depletion. We therefore created the strain GM3880 with the $Cori_{UP}$ mutation placed at the natural *Cori* chromosome position but which is otherwise identical to GM3817 used above in Figure 2. By using GM3880 in

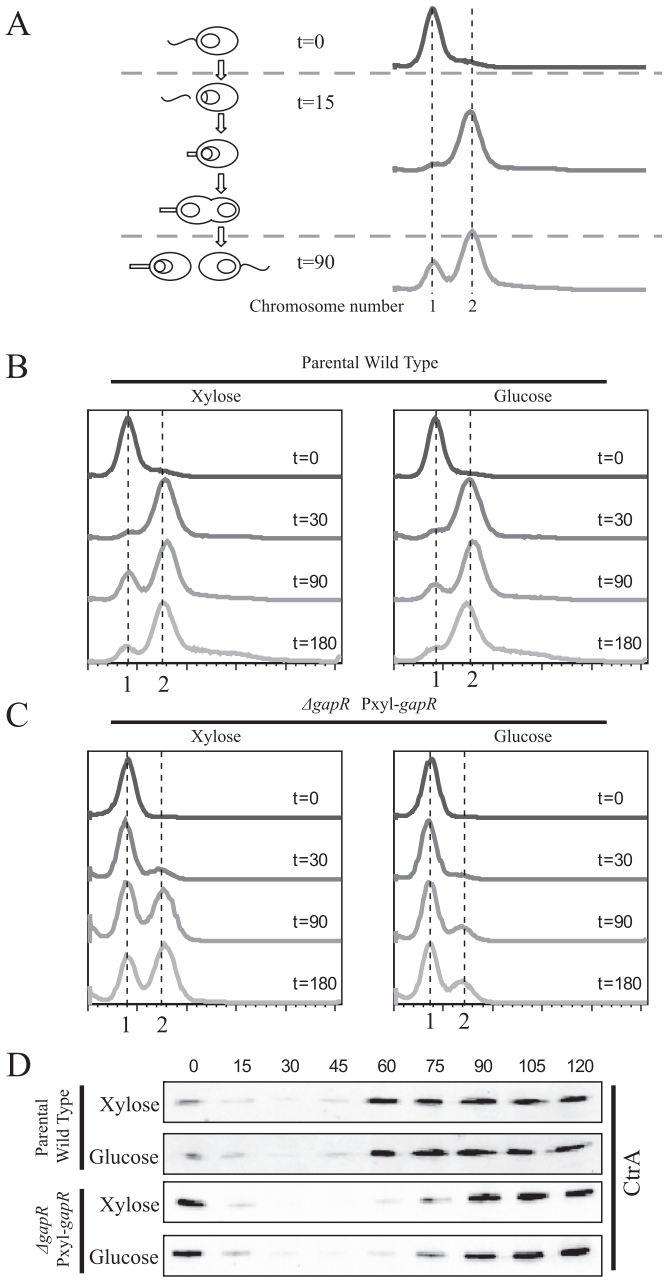

Figure 2. Cells with insufficient GapR fail to initiate chromosome replication. (**A**) Presentation of the flow cytometry-based assay to measure initiation times of chromosome replication. A synchronized culture of WT strain GM1609 proceeds through the cell cycle (cartoon on left) developing from swarmer cells (top) to stalked cells, predivisional cells, and finally asymmetrically divided cells (bottom). Flow cytometry was used to distinguish cells with replication versus non-replicating chromosomes. Cultures were sampled at progressive times and transferred into media with antibiotics that block further replication initiation and cell division while allowing ongoing replication to continue and produce two chromosomes (see Materials and Methods). Flow cytometry assess fluorescent chromosome DNA versus cell numbers (traces on right). Prior to initiation, $t = 0$ cells contain one chromosome, while after initiation $t = 15$ min cells contain two chromosomes. (**B** and **C**) Initiation time experiments in synchronized cultures of the parental WT strain (GM1609; B) and the GapR Pxyl conditional-expression strain (GM3817; C) assessed using flow cytometry as outlined in (A) and grown in media containing xylose (left histograms; GapR expression induced) or glucose (right histograms; GapR expression not induced). Samples were taken at the indicated times (minutes). (**D**) Immunoblots for CtrA master regulator protein. Samples were taken at time points indicated above the lanes (minutes) from synchronized cultures in (B) and (C). CtrA patterns confirm microscopic observations and show that the cell cycles, with respect to early cell differentiation, proceeded normally and were not influenced by the xylose versus glucose media conditions. The delayed replication response seen here in 2C Glucose was replicated in two additional experiments not shown.

the otherwise same replication timing experiment, we now see that the $Cori_{UP}$ mutation advances replication and the severe replication timing lag is no longer seen in glucose media (compare flow cytometry results in Figure 2 with Supplementary Figure S4A).

Similarly, if increased GapR binding to *Cori* is driving the extra *Cori*-plasmid replication of $Cori_{UP}$ seen in Figure 1B, then genetically removing GapR should remove the differential replication of the $Cori_{WT}$ and $Cori_{UP}$ sequences. To test this prediction, we isolated a spontaneous suppressor strain which retained viability despite lacking *GapR* (GM3875; see Supplementary Methods). Repeating the autonomous replication assays confirmed that the ~2-fold differential replication between the $Cori_{WT}$ and $Cori_{UP}$ *Cori*-plasmids seen in WT GM1609 is no longer seen in GM3875 (Supplementary Figure S4B).

In vitro GapR has broad DNA-binding specificity like nucleoid-binding proteins

EMSA experiments show that GapR has high affinity ($K_d \sim$ 10 nM) for *Cori* DNA and that GapR probably binds DNA through very specific peptide contacts, because an GapR mutation (Y82A) at its conserved tyrosine abolishes all high affinity EMSA binding to *Cori* (Supplementary Figure S6). GapR clearly has DNA sequence preferences (Figure 1) and we sought to identify GapR binding sites inside *Cori*, as we did for other *Cori* regulatory proteins (7), through *in vitro* DNase I protection ('footprint') experiments. Therefore, purified histidine tagged GapR protein (as in Figure 1D) was added to 32-P end-labeled WT *Cori* DNA. However, we did not see DNase I protection until a threshold concentration of GapR protein produced complete protection over the *Cori* DNA shown in Figure 1A (data not shown). Such results were repeated under a range of *in vitro* conditions and they imply that the intrinsic DNA-binding specificity of GapR is broad and relatively non-selective. However, since GapR selectively affects *Cori* replication *in vivo* (Figures 1B, and 2, Supplementary Figure S4A, S4B), we reasoned that additional 'extrinsic' factors must direct GapR to *Cori* and that clues can be found through whole genome binding studies.

In vivo GapR has broad genomic DNA-binding specificity but with specific peak distributions

We used chromatin-immuno-precipitation and Illumina sequencing (ChIP-seq) to determine how GapR is distributed on the *C. crescentus* chromosome in growing WT cells. To show that ChIP-seq specifically identifies true GapR binding positions, we performed the same analysis on the *ΔGapR* GM3875 'suppressor strain' that survives without

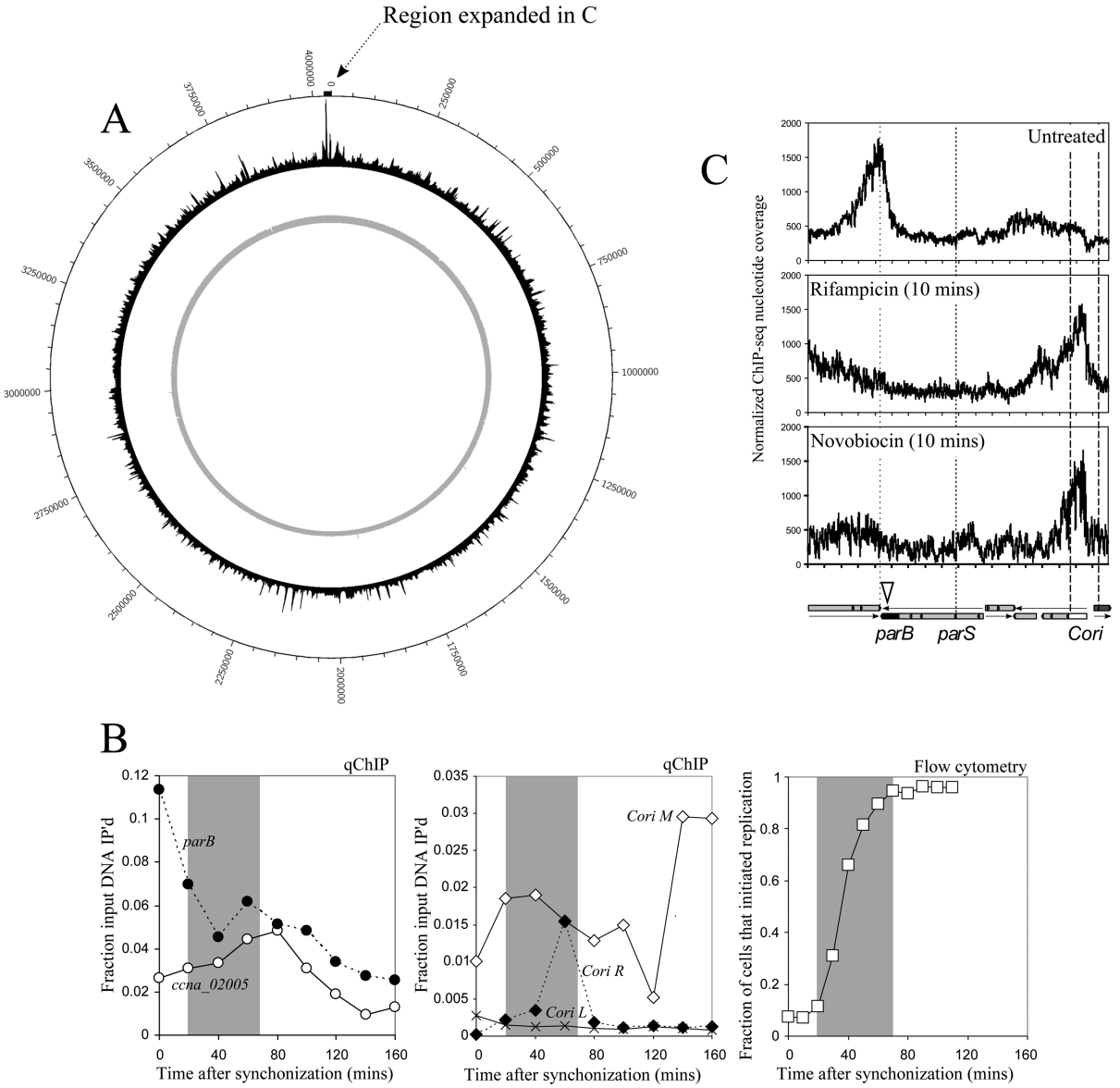

Figure 3. Genome binding distributions of GapR. (**A**) The circular *C. crescentus* chromosome aligned with two whole-genome ChIP seq signals (175 bp resolution histogram bins representing % of total reads) using the GapR anti-serum first on the WT strain (NA1000, black outer signal) and then the Δ*GapR* suppressor strain (GM3875, grey inner signal). The standard bp positions of the WT NA1000 genome are displayed in the outer circle, with the small black bar above the 0-position indicating the region that is expanded in (C). (**B**) qChIP (GapR anti-serum) analysis performed on synchronized WT GM1609 cells grown in M2G media. GapR binding was measured by qPCR at the following positions: at *parB* (left panel; filled circles, dashed line), at *ccna_02005* (left panel; open circles, solid line), and at three positions in *Cori* (middle panel, see Figure 1A for positions of probes: Cori L, crosses, solid line; Cori M, open diamonds, solid line; Cori R, filled diamonds, dashed line). The grey window shows the cell cycle period during which 95% of the chromosomes initiated replication, as measured by flow cytometry (right panel; see Figure 2A and Materials and Methods). (**C**) ChIP-seq signals over the region surrounding *parB* and *Cori* from untreated WT NA1000 cells (top trace) and from the same culture sampled and treated for 10 min with 30 ug/ml rifampicin (middle trace), or 100 ug/ml novobiocin (bottom trace). In the schematic below these three ChIP seq signals, the genetic organization in this region is shown with the *parB* gene indicated in black, and *hemE* and *ccna_00001* which flank *Cori* indicated in white and dark grey respectively. The *Cori* region (the *Bam*HI fragment that defines the autonomously replicating *Cori*) is indicated by vertical dashed lines (long dashes), the position of *parS* by one vertical dashed line (short dashes) and the position of the intergenic region downstream of *parB* by a vertical dotted line. The white vertical arrowhead indicates the position of the *parB* primers used for the qChIP analysis in (B). Note that (A) and (C) represent data from whole-genome ChIP-seq experiments on independent cultures and that both experiments position the most relevant GapR peaks (Supplementary Figure S7A) at the same locations.

GapR. This comparison confirmed the high specificity of our GapR anti-serum, because none of the prominent WT peaks are present in the *ΔGapR* GM3875 control (Figure 3A; compare outer Circos black trace with inner grey trace). This ChIP-seq analysis also argued for weak DNA sequence specificity since these GapR peaks are broad, often spanning whole genes (e.g. see Figure 3C) and they lack distinct boundaries.

Interestingly, the first ranked GapR peak was found over the chromosome partitioning gene *parB* (end of the *parABS* operon) in two independent ChIP seq experiments (Figure 3A and in C 'Untreated') and we confirmed this abundant GapR binding at *parB* and other key positions using ChIP and qPCR (Supplementary Figure S5A). We attempted to identify DNA sequences under this and other top ranked peaks using the MEME software suite (12). While this sequence alignment approach has identified DNA binding sites with similar ChIP-seq data (13), we did not find DNA motifs that accounted for the GapR distributions on the chromosome. Nonetheless, GapR does show a weak 'intrinsic DNA specificity' based on its association with degenerate DNA motifs which we address further below.

Antibiotic treatments rapidly redistribute GapR peaks

We considered what 'extrinsic' factors might direct GapR into prominent peaks, thereby overcoming GapR's weak 'intrinsic specificity' for DNA. Growing cells are engaged in replication, transcription and coupled translation and such macromolecular syntheses, each driven by large molecular machines, might move and reposition GapR. We therefore tested ChIP-seq signals from WT growing cultures and from cultures split and treated with rifampicin or with novobiocin. We saw that most GapR binding peaks were eliminated after 10 min with either treatment, as for example the peak at *parB* (Figure 3C).

Novobiocin and rifampicin redistribute GapR to the *hemE/Cori* replication locus

Interestingly, a new prominent peak over the left side of *Cori* and within the *hemE* gene, was created after either novobiocin or rifampicin treatments (Figure 3C). This observation is very significant, because *hemE* transcription and *Cori* replication are interrelated and this DNA uniquely supports autonomous replication (14). To confirm this result, we performed qChIP experiments with these same antibiotics. While ChIP-seq reports relative amounts of binding, our qChIP experiments demonstrated that the absolute amount of GapR binding to *Cori* at *hemE* increases following either novobiocin or rifampicin treatments (Supplementary Figure S5B).

The significance and uniqueness of GapR peaks at *parB*, *hemE/Cori* versus other loci

The preceding observations and especially GapR binding at *parB* and *hemE/Cori* are potentially very significant for cell cycle studies. This consideration prompted us to more rigorously test the significance of these peaks in our ChIP seq experiments. Here we summarize the details provided in our supplementary data: We analyzed the whole genome ChIP seq data set (partially presented in Figure 3C). For the 'untreated' growing cells we identified 36 GapR relevant peaks (according to the cutoff criteria described in Supplementary Figure S7). These same 36 peaks are reproducible since they are all present among the top 80 GapR relevant peaks from the independent ChIP seq experiment presented in Figure 3A, and most significantly, *parB* is the first GapR relevant peak in both experiments.

The short 10 min antibiotic treatments with rifampicin (Rif) or with novobiocin (Novo) leveled the genome-wide distribution of GapR. While 36 GapR relevant peaks were seen in the untreated culture, only three GapR +Rif relevant peaks and only seven GapR +Novo relevant peaks satisfied the same cutoff criteria (Supplementary Figure S7ABC). None of the 36 GapR relevant peaks were found among the GapR +Rif and GapR +Novo peaks (Supplementary Figure S7DE). Therefore, these GapR peaks that characterize growing cells, including *parB*, result from activities inhibited by either antibiotic, suggesting that active replication and transcription and their consequences, e.g. molecular collisions and/or DNA supercoiling work to actively maintain these 36 peaks. Interestingly, despite the overall more even GapR distribution created by Rif and Novo, the one common relevant peak produced by both Rif and Novo treatments is at the *hemE/Cori* locus (Figure 3C, Supplementary Figure S7F). Therefore, this last result suggests a relationship between *Cori* and GapR that is unique among the whole genome.

GapR binding correlates with the initiation of chromosome replication and partitioning

Since *parB* is located within 10 kb of *Cori* and since both loci have essential cell cycle roles, we further examined GapR binding during the cell cycle with qChIP experiments on synchronized WT cells (Figure 3B). Using qChIP primers at *parB* this signal peaked early in the cell cycle immediately preceding the *Sw* to *St* cell transition and the initiation window for chromosome replication (20–60 min Figure 3B). The first ranked *parB* timing contrasted with the second ranked GapR binding region, at *ccna_02005* close to the terminus, which peaked much later at ∼80 min in to the cell cycle. We also examined GapR binding at three positions spanning *Cori* (Figure 1A; asterisks). *Cori* L binding proximal to *hemE* was weak and showed no cell cycle variation. In contrast, at *Cori* M binding to the middle of *Cori* was much stronger and this signal doubled during the initiation window for replication and again late in the cell cycle prior to the next round of replication initiation that starts after cell division. In contrast to these patterns, GapR binding to *Cori* R, close to the *in vitro* EMSA target in Figure 1CD, peaked most discretely at 60 min, during the latter half of the initiation window for replication (Figure 3B). Therefore, GapR binding changes significantly during the cell cycle: GapR binding inside *Cori* correlates with the initiation of chromosome replication and the distinct *Cori* L M R binding patterns during replication initiation suggest specialized roles and interactions with different replication proteins. Interestingly, peak GapR binding at *parB* precedes chromosome duplication and separation and yet remains

high, suggesting early roles before and during chromosome partitioning that we discuss further below.

Microscopy shows that GapR is dynamically repositioned during chromosome partitioning

C. crescentus chromosome partitioning has been studied in *gfp-parB* strains where the GFP-ParB fusion protein binds the *parS* (centromere-like) locus near *parB* and *Cori* to form fluorescent foci at the cell poles (15). We fused the mCherry protein to the N-terminus of GapR and integrated this construct at P*xyl* in strain GM3905 (*gfp-parB*) to create strain GM3921 (*gfp-parB Pxyl::mCherry-GapR*). This mCherry-GapR protein is induced by xylose and it retains important *in vivo* functions, as GM3921 derived strains remained viable when the native *GapR* gene was deleted (see Supplementary Table S1). Therefore mCherry-GapR localization probably reports the native GapR localization. We synchronized GM3921 cells and observed how the mCherry-GapR distribution changed (Figure 4 and Supplementary Figure S8). In $t = 0$ *Sw* cells, mCherry-GapR initially distributed as a gradient with its peak very near but not overlapping the flagellated cell pole marked by the single GFP-ParB focus. As chromosome replication and partitioning initiated, in $t = 15$ and $t = 30$ *St* cells, one GFP-focus remained polar while one GFP-focus moved away and the mCherry-GapR peak moved with this partitioning GFP-ParB focus (peaks of GFP and mCherry fluorescence co-localized in 76% of partitioning cells at $t = 15$). This movement created a wider mCherry-GapR free gap between the polar GFP-focus and the partitioning GFP-ParB focus (seen in 94% of partitioning cells at $t = 15$). The GFP-ParB focus then passed through the peak of the mCherry-GapR gradient as it moved further away to the opposite pole. Finally in $t =$ 90 pre-divisional cells, mCherry-GapR established a separate gradient in each nascent cell compartment, with a peak of mCherry-GapR close to, but separated from, each pole marked by its GFP-ParB focus.

Strategies to test if chromosome partitioning is a dominant cell cycle role for GapR

Since chromosome partitioning requires *parS* site duplication and GapR depletion blocks replication (Figure 2), we could not use the same GapR depletion strategy and track GFP-ParB foci during the cell cycle. As our first strategy, since we could not study partition during the short ∼40 min *Sw* to *St* cell cycle window, we used prolonged GapR depletion times instead. Accordingly, we constructed *gfp-parB* strains GM3905 *gfp-parB* and GM3918 *gfp-parB ΔGapR Pxyl::GapR* corresponding to the WT and regulated *GapR* expression strains used in Figure 2. Prolonged GapR depletion experiments, e.g. GM3918 cells 16 h PYE with glucose, allowed many cells to finally initiate chromosome replication and as expected, these cells had extra misplaced GFP-ParB foci (data not shown). However, we could not draw firm conclusions, because such GM3918 cells also showed cell division defects. As a broad-binding protein, it is also likely that GapR depletion impacts many functions that cumulatively produce unpredictable consequences, especially since such cells lose viability during the prolonged shut-off period (Supplementary Figure S2B).

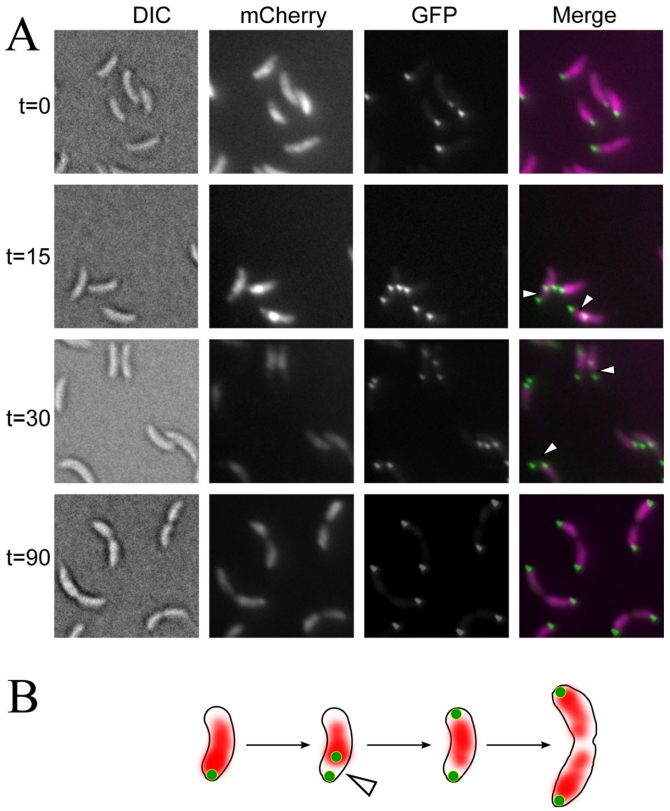

Figure 4. GapR distribution changes during cell cycle progression and correlates with chromosome *parS* movements. (**A**) Microscopy images from a synchronized culture of GM3921 (*gfp-parB Pxyl::mCherry-GapR*) taken at $t = 0$, $t = 15$, $t = 30$ and $t = 90$ (minutes). A larger set of images is presented in Supplementary Figure S8. At each time-point we imaged >400 cells. Representative fields viewed with DIC, mCherry and GFP channels are shown in black and white and the merged mCherry/GFP channels are colored (pink and green respectively). The arrowheads in the merged $t = 15$ and $t = 30$ pictures mark cell regions between the two GFP-ParB foci that (compared with $t = 0$ cells) become exceptionally free of mCherry-GapR. In these cells the peak mCherry-GapR fluorescence often co-localizes with the partitioning GFP-ParB focus. (**B**) A cartoon summary of inferred GFP-ParB and mCherry-GapR movements over the cell cycle from *Sw* cell ($t = 0$, left) to pre-divisional cell ($t = 90$, right). As in (A) the arrowhead marks the sub-cell region between two GFP-ParB foci that becomes cleared of mCherry-GapR as both fluorescence signals move together at this early phase of the cell cycle.

As our second strategy, we took advantage of the viable *ΔGapR* suppressor strains (described in supplementary data). As we noted, while the initial removal of GapR is lethal, the *ΔGapR* suppressor strains that survive resemble WT cells. We reasoned that the most dominant roles, such as perhaps chromosome partitioning would be the most difficult to compensate and therefore only partially suppressed in these *ΔGapR* strains. Also, we selected a suppressor strain with normal replication kinetics during the most relevant *Sw* to *St* cell differentiation period (Supplementary Figure S4C). This strain allowed us to observe GFP-ParB/partitioning independently from chromosome replication.

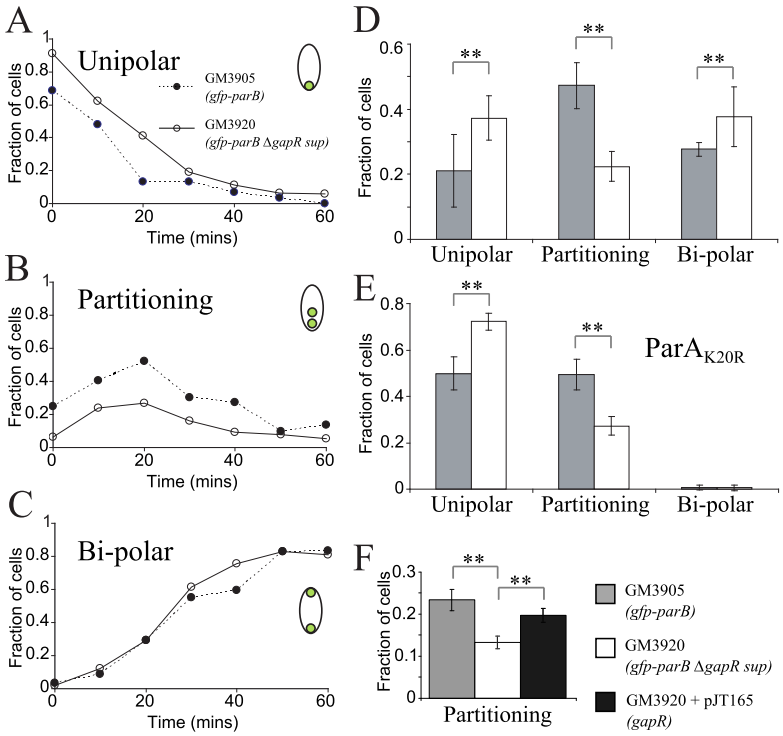

Figure 5. *ΔGapR* cells are specifically defective in the early phase of chromosome partitioning. (**A**–**C**) Quantification of cells at three stages of chromosome partitioning in synchronous cultures of WT cells carrying a chromosomal *gfp-parB* (GM3905; filled circles, dotted lines) and in a *ΔGapR* suppressor strain with the same chromosomal *gfp-parB* fusion (GM3920; empty circles, solid lines). Over the first 60 min of synchronous growth, these graphs show the changing fraction of cells that had a single GFP-ParB focus, i.e. 'Unipolar' stage (A), a partially partitioned pair of GFP-ParB foci, i.e. 'Partitioning' stage (B) and cells that had completed partitioning, i.e. 'Bi-polar' stage with a pair of polar GFP-ParB foci (C). $n > 100$ cells were scored for each time point. (**D**) Quantification of cells at each of the three stages of chromosome partitioning, as depicted in (A–C) and scored at the $t = 20$ min time-point. Data from three independent synchronous cultures of GM3905 (gray bars) and GM3920 (white bars). $n > 300$ cells were scored for each stage. (**E**) As in (D), quantification of cells at each of the three stages of chromosome partitioning depicted in (A–C) and scored at the $t = 20$ min time point of synchronous cultures. Strains GM3905 (gray bars) and GM3920 (white bars) carried a chromosomal integrated P*van-parAK20R* plasmid. ParAK20R protein expression was induced with vanillate two hours prior to synchronization and this treatment blocks ParA-mediated chromosome segregation, as shown by the absence of cells in the 'Bi-polar' stage. (**F**) Quantification of cells at the 'Partitioning' stage sampled at $t = 25$ min from synchronous cultures of GM3905 (gray bar), GM3920 (white bar) and GM3920 + pJT165 (plasmid carrying *GapR* under its native promoter; black bar). For D–F, $n > 300$ cells were scored for each condition. Significant differences ($P < 0.01$, z-test) are indicated by **.

Early-phase partitioning is assisted by GapR

According to the preceding strategy, we compared synchronous cultures of the *gfp-parB ΔGapR* suppressor strain (GM3920) with the *gfp-parB* parental strain (GM3905) and we quantified 3 types of GFP-ParB localization patterns ('unipolar', 'partitioning' and 'bi-polar' patterns, Figure 5ABC) at progressive cell cycle times. GM3920 consistently showed more unipolar (Figure 5A) and fewer partitioning GFP foci (Figure 5B) during the early 0–40 min cell cycle period. These differences reflect early partitioning defects, because they are too large to be caused by delayed chromosome replication in *ΔGapR* GM3920 versus WT GM3905. As controls, these same cultures when spotted for microscopy were also sampled for the replication run-out assay (as done in Figure 2). For all samples the fraction of replicating cells was practically the same and the differences between GM3920 and GM3905 were always <10%. Interestingly, the bi-polar GFP-ParB foci appeared at the same rate in both synchronized cultures (Figure 5C), suggesting that despite early differences both *ΔGapR* the WT strains have equally efficient means to pull the GFP-ParB foci to their ends. Therefore, to confirm these results we next focused on the early partitioning period; we repeated these synchronized culture experiments in triplicate and examined cells at the 20 min time point. This fixed time analysis (Figure 5D) confirmed the time-course analysis (Figure 5A–C) and demonstrated that GM3920 cells without GapR have a deficit of 'partitioning', i.e. double-foci cells during the early phase of partitioning.

Genetic analysis also implicates *GapR* in early phase partitioning without ParA activity

The late phase of chromosome portioning requires ParA activity while the early phase does not (16). To confirm that the defect in GFP-ParB/*parS* separation of GM3920 occurs during the early ParA-independent phase of chromosome segregation, we blocked ParA-mediated chromosome partitioning by expressing the dominant negative allele ParA$_{K20R}$ in synchronized cultures prior to the microscopic analysis at the 20 min time point. As expected (16), expression of ParA$_{K20R}$ abolished bi-polar localization of GFP-ParB foci (Figure 5E) that requires ParA. How-

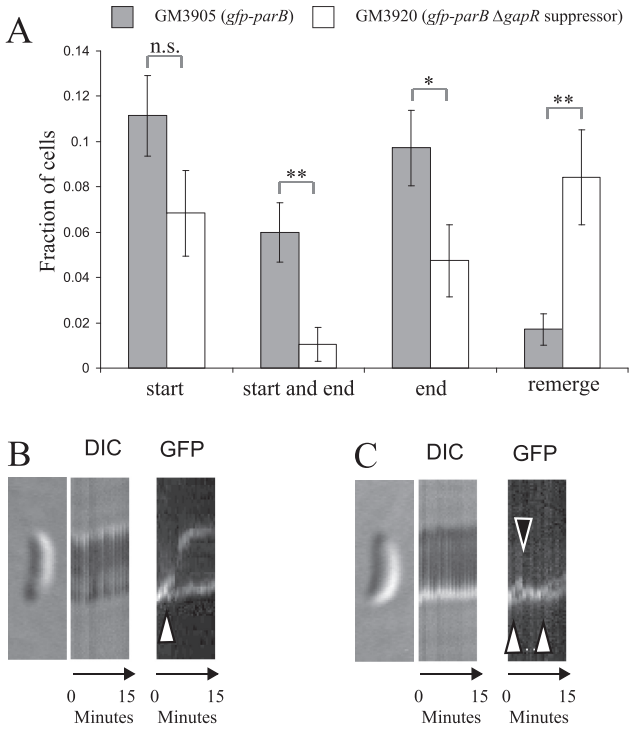

Figure 6. Time-lapse microscopy shows that GapR aids the early phase of chromosome partitioning. (**A**) Quantification of the partitioning events of GM3905 (WT, gray bars) and GM3920 cells (*ΔGapR*, white bars) over a 15 minute time-course assayed by time-lapse microscopy. Cells were counted and classified according to whether they started partitioning ('start'; one polar GFP focus becomes two), completed partitioning ('end'; one polar and one mid-cell GFP focus become two bi-polar foci), both started and completed partitioning ('start and end'; one polar GFP focus becomes two bi-polar foci) or underwent a 'remerge' event (two foci combined to show one focus) over the 15 minutes of time-lapse microscopy. Error bars indicate the estimated standard deviation of a Poisson distribution ($n = 350$ and 190 for GM3905 and GM3920 respectively). Significant differences have probabilities (z-test) of $P < 0.05$ and $P < 0.01$, indicated by * and ** respectively. No significant difference (n.s.) $P > 0.05$. (**B** and **C**) Single-cell kymographs created from sliced and aligned time-lapse images, taken every minute over 15 minutes. Examples of GM3905 (B) and of GM3920 (C) cells undergoing a complete 'start and end' partitioning (B) and of a 'remerge' partitioning (C) of GFP-ParB foci. To the left of the DIC kymograph, the first whole cell image is indicated to show pole positions (note some drift in cell position during the experiment). White arrowheads in the GFP kymographs indicate separation events where two GFP-ParB foci became resolvable. The black arrowhead in (C) indicates a 'remerge' event where two GFP-foci fused into one foci. These images therefore illustrate the most significant 'start and end' (B) and 'remerge' (C) events quantified in (A).

ever, the deficit of 'partitioning' GFP-ParB foci remained in GM3920 when ParA was blocked (Figure 5E), thereby placing the cause of this deficit in the early ParA-independent phase of chromosome partitioning.

Because we examined chromosome partitioning in a suppressor strain rather than in a simple *ΔGapR* strain, we sought to confirm that the early partitioning deficit in GM3920 results from the lack of GapR rather than from a suppressor mutation. We therefore transformed GM3920 with pJT165, carrying *GapR* under its native promoter to complement the *GapR* deletion, and we assayed chromosome partitioning as in Figure 5DE. pJT165 ameliorated the partitioning deficit of GM3920 (Figure 5F), further showing that GapR directly aids the early phase of chromosome partitioning.

Time-lapse microscopy further implicates GapR during the earliest *parS*/centromere separation

To investigate what caused the deficit of 'partitioning', i.e. fewer double GFP-ParB/*parS* foci in the *ΔGapR* cells, we performed time-lapse microscopy on single cells of synchronized cultures. Swarmer cells were isolated and after 10 minutes of synchronous growth in PYE liquid, cells were transferred to nutrient PYE/agar pads on microscope slides for a 15 min time-lapse analysis of GFP-ParB foci. During this cell cycle window, we observed and quantified 4 categories of foci movements: First, we observed that fewer "start' events (one polar focus becoming two close foci) for GM3920 cells compared to control GM3905 cells (Figure 6A). Second, we observed fewer 'start and end' events (one polar focus becoming two complete bipolar foci) for GM3920 cells (Figure 6A, with a specific example in Figure 6B). Third, we also observed fewer 'end' events (two close foci becoming completely bipolar) for GM3920 cells. Therefore, all of these observations independently support defective partitioning *ΔGapR* cells.

The fourth category of foci movements was most informative. We observed significantly more 'remerge' events (two close GFP-ParB foci combining into one focus) for *ΔGapR* GM3920 cells (Figure 6A, with a specific example in 6C). These 'remerge' events probably account for the deficit of separated GFP-ParB foci in GM3920 that we scored as 'partitioning' foci in Figure 5BDE and they would also give a false impression of defective replication scored as 'unipolar' foci in Figure 5A. We interpret a 'remerge' event as a failure to maintain the first separation step of chromosome partitioning. This defective event coincides with the symmetry-splitting 'discrimination' function of the *par* system that keeps one *parS* locus at the *St* pole and that sends the other *parS* locus to the emerging *Sw* pole. To the best of our knowledge, such *parS* remerging events have not been reported before, probably because they are rare in WT cells (Figure 6A) and the small separation is difficult to observe (Figure 6C). 'Remerge' events only become apparent in our *ΔGapR* cells when the early partitioning phase is closely examined.

DISCUSSION

We first proposed that GapR was a DNA sequence-specific regulator of *Cori* but further studies caused us to modify this hypothesis. For example, the broad DNA-binding specificities and dynamic peak distributions, argue that GapR should instead be classified as a nucleoid associated protein (NAP) that potentially impacts the whole genome. Interestingly, genome-wide surveys confirmed that GapR has unique associations with the *hemE*/*Cori* and the nearby *parABS* loci and we gathered evidence for GapR's expanded roles. While GapR lacks strong DNA sequence-specificity, it does act as a regulator. We propose that GapR is best described as a facilitator of complex regulatory processes and specifically of the initiation of chromosome replication and of the initiation of chromosome partitioning. Regulators optimize essential processes and need not be essential

themselves. Accordingly, GapR is essential for normal rapid growth and while we could isolate *ΔGapR* strains, these strains always grew slower and progressed less efficiently through the cell cycle. We specifically isolated one *ΔGapR* suppressor strain that appeared to sufficiently restore the cell cycle program during the *Sw* to *St* cell transition so that, at least under standard rich media conditions, these cells looked normal and initiated chromosome replication with normal timing. However, closer examinations revealed that this *ΔGapR* strain had less efficient chromosome separation and partitioning, emphasizing GapR's dominance in this process.

During our studies on GapR (http://biorxiv.org/content/early/2016/12/04/091496), two independent groups also began studying the same *C. crescentus* gene/protein (CCNA_03428), reported as GapR (17,18). Accordingly, we changed our earlier designation of *opaA* (origin and partition binding protein A) to match this recent literature. Unlike our replication function-based approach (Figure 1), both groups started from a bioinformatics survey of essential genes (11). In agreement with our conclusions, both groups presented GapR/OpaA as a NAP that participates more directly in the dimorphic cell cycle of *C. crescentus* than previously studied NAPs. For example, both groups reported that GapR/OpaA has subtle yet global impacts on genetic transcription, although they differed on the identity of the genes and their significance for the cell cycle. Most pertinent to our results, while the first report by Ricci *et al.* attributes GapR/OpaA distributions on the chromosome primarily to preferential DNA-binding to AT-rich DNA (17), the second report by Arias-Cartin *et al.* (18) deemphasizes the importance of specific DNA-binding sequences. Instead, Arias-Cartin *et al.* proposed a dynamic binding model whereby replication forks dislodge DNA-bound GapR/OpaA proteins which then preferentially rebind to the replicated DNA.

How does GapR in fact bind genomic DNA and how can we explain these contradictions?

We observed a dynamic repositioning of GapR/OpaA by DNA-protein crosslinking (Figure 3) and fluorescence microscopy (Figure 4). GapR/OpaA binding distributions change rapidly after antibiotic treatments (Figure 3AC, Supplementary Figures S7, S9, S10) and during the course of normal cell cycle progression (Figures 3 and 4, Supplementary Figure S8). According to Arias-Cartin *et al.*, replication forks starting from *Cori* create an GapR/OpaA gradient peaking at *Cori*, because this region has more time to rebind the displaced protein (18). Their observations are potentially consistent with our microscopic observations (Figure 4), because in $t = 0$ *Sw* cells we also see mCherry-GapR gradients decreasing from the *parS*/ParB-GFP polar foci, and in $t = 15$, $t = 30$ cells we see mCherry-GapR receding from these poles, producing a fluorescence gap that could be caused by replication forks displacing mCherry-GapR. However, replication fork interactions alone cannot explain local GapR/OpaA peaks, nor can they explain their rapid and local cell cycle variations (Figure 3B). We see that transcription and translation also reposition GapR/OpaA. Regarding our ChIP seq experiment from Figure 3C, we see that blocking RNA polymerase evens the genomic distribution of GapR/OpaA, since a 10 min +Rif treatment leaves only three relevant peaks (above the cutoff) compared with the 'untreated' 36 relevant genome-wide peaks (Supplementary Figure S7). However surprisingly, a 10 min chloramphenicol (+Chl) treatment of this same culture sharpens the genomic distribution of GapR/OpaA and now produces 81 relevant peaks (Circos Supplementary Figures S9B and S10B). This is a very significant redistribution considering that only 2 of these +Chl relevant peaks overlap the 'untreated' 36 GapR peaks and interestingly one of these overlap peaks is *parB*, yet another unexpected connection between GapR/OpaA and chromosome partitioning.

Further regarding the genetic contexts of GapR/OpaA peaks, we see that like the peak over the end of *parB*, ∼80% of the 'untreated' 36 peaks position where two genes/operons converge (Supplementary Figure S10E). In contrast, over 80% of the GapR +Chl 81 relevant peaks position over upstream genetic regions which are often AT-rich. Plotting genome-wide peak ranking versus GC content confirms that +Chl creates the most relevant peaks that are AT-rich (compare Supplementary Figure S10F and G). These observations probably have regulatory significance as antibiotics or similar stresses that block translation would rapidly direct GapR/OpaA to AT-rich promoters and thereby alter genetic transcription.

While our ChIP seq experiments analyzed natural GapR/OpaA protein, both recent reports used genetic/protein fusions for ChIP seq and other analyses (17,18). We argue that such gene/protein fusions cause artifacts and misleading conclusions. For example, Ricci *et al.* (17) proposed that GapR/OpaA binds preferentially to AT-rich promoters thereby 'fine-tuning' genetic transcription of cell cycle genes. However, Ricci *et al.* used a FLAG-GapR fusion and we therefore reanalyzed their primary ChIP seq data with our criteria. Accordingly, we see 474 FLAG-GapR relevant peaks and therefore a much sharper and focused genome-wide distribution than our natural GapR/OpaA with only 36 relevant peaks (compare Supplementary Figure S10C and S10A). Noting that the chloramphenicol treatment (+Chl) also sharpened and focused GapR/OpaA distributions, we see that 73 out of our 81 relevant +Chl peaks overlap with the 474 FLAG-GapR peaks, while only 8 out of our 36 'untreated' GapR relevant peaks show an overlap (Supplementary Figure S10D). Furthermore, like the +Chl peaks, the highest ranking FLAG-GapR peaks show a very similar bias towards AT-rich DNA (compare Supplementary Figure S10G and S10H). We conclude that the FLAG-GapR fusion mimics chloramphenicol stress and that all experiments with GapR fusions should be interpreted with care. Nonetheless, the redistribution of GapR to AT-rich DNA, including to *parB* and *Cori* loci (Supplementary Figure S10D) is significant and probably reflects a weak intrinsic DNA sequence bias suggested by specific AT-rich motifs (Supplementary Figure S10IJK). While our studies on chromosome replication and partitioning focused on non-stressed cells growing under optimal conditions, it is likely that GapR also responds to stresses and that GapR helps regulate stress-response genes, a hypothesis also suggested by Arias-Cartin *et al.* (18). We also speculate

that GapR binds and perhaps protects AT-rich DNA, because we observe that the $Cori_{UP}$ mutant DNA is more AT-rich and this promotes what appears to be GapR protein oligomerization (higher multimeric EMSA shifts in Figure 1D).

How is GapR involved in chromosome replication?

We initially purified GapR by its EMSA binding to specific *Cori* DNA and we proposed that GapR regulates chromosome replication, because increased GapR binding to $Cori_{UP}$ mutant DNA *in vitro* correlates with increased autonomous replication of $Cori_{UP}$ mutant plasmids *in vivo* (Figure 1). Subsequent experiments support a chromosome replication hypothesis. For example, our genetic shut-off experiments show that lack of GapR selectively prevents the initiation of chromosome replication *in vivo* (Figure 2). We scrutinized the consequences of *gapR* shut-off over the short-term 90 min period of the *C. crescentus* cell cycle. These are *in vivo* protein depletion experiments, because GapR is an abundant and stable protein (data not shown). Therefore, we actually observed the consequences of reduced GapR protein levels. Under these conditions and as in WT cells, swarmer (*Sw*) cells differentiated into stalked cells (*St*) which then divided asymmetrically. The CtrA master regulator marks the *Sw* cells and its disappearance marks the development of *St* cells while its reappearance (new synthesis) marks the onset of asymmetric cell division (19,20). Therefore, it is very significant that CtrA degradation kinetics are not changed by GapR depletion while the initiation of chromosome replication is severely retarded in the *GapR* shut-off cells (Figure 2). We also presented two supplementary experiments (Supplementary Figure S4) demonstrating that GapR acts directly at *Cori*. Therefore, lack of GapR selectively inhibits chromosome replication, while the general program of *Sw* to *St* cell differentiation proceeds normally.

Interestingly, GapR protein levels increase during the cell cycle, and compared to *Sw* cells GapR concentrations are at least 2-fold higher in late dividing *St* cells (Supplementary Figure S11). Therefore, bulk GapR protein concentrations are asymmetrically distributed by cell division and *Sw* cells receive lower concentrations of GapR than *St* cells. However, GapR protein concentrations alone do not determine DNA-binding. When GapR concentrations are low, substantially more GapR binds to the *parABS* DNA of synchronized *Sw* cells (Figure 3B). Also, GapR binds to *Cori* with very specific spatial and temporal patterns (Figure 3B, compare *Cori* L, M and R patterns). *Cori* is a platform for many protein interactions. Therefore, these GapR binding kinetics presumably reflect the many replication protein interactions that occur during synchronized chromosome replication.

How is GapR involved in chromosome partitioning?

C. crescentus chromosome partitioning is bi-phasic, with an initial slow separation of ParB-*parS* complexes (16) followed by a rapid movement of one ParB-*parS* complex to the new cell pole (21). Only the rapid second phase of partitioning requires ParA ATPase. Blocking ParA activity by expressing the dominant-negative allele $ParA_{K20R}$ abolishes final *parS* placement at the distant cell pole (16,21). Nevertheless, these $ParA_{K20R}$ cells still undergo the initial slow and partial separation of ParB-*parS*. Our microscopy studies showed that significantly fewer cells separate the ParB-*parS* complexes in the *ΔGapR* suppressor strain and our experiments placed the separation defect in the initial ParA-independent phase of chromosome partitioning. Additionally, time lapse microscopy showed that fewer *ΔGapR* suppressor cells separate their ParB-*parS* complexes and that a greater proportion of them remerge. Therefore, the initial separation of the *par*-*Cori* region is not maintained and GapR may supply or help direct a driving force for this separation.

The dynamic cellular mCherry-GapR distributions (Figure 4, Supplementary Figure S8) also argue that GapR acts during the initial slow separation phase. Interestingly, the strongest mCherry-fluorescence stops next to the GFP-ParB/*par*S focus in the $t = 0$ *Sw* cells (e.g. Supplementary Figure S8C). Subsequently, two GFP-ParB/*par*S foci form and one focus follows the mCherry-fluorescence as it recedes away from the cell pole still occupied by the remaining focus ($t = 15$, $t = 30$ cells). These mCherry-GapR movements do not use ParA and they suggest a quasi-mitotic process. At later times, the GFP-ParB/*par*S focus stops following and instead moves through the main mCherry-GapR fluorescence on its way to the opposite cell pole. This movement into the mCherry zone probably reflects a transfer from the early/slow GapR-system to the later/fast ParA-system.

The motor for the early phase of chromosome partitioning is unknown (16) and previous studies have suggested that RNA polymerase, DNA replication and bulk polymer properties may drive these movements (22–24). Inhibitors of these polymerases affect GapR binding at *parB* and noting that the receding edge of mCherry-GapR coincides with the moving GFP-ParB/*par*S focus (Figure 4 and Supplementary Figure S8 $t = 15$, $t = 30$), we propose that replication forks may not only displace GapR/OpaA (18) they may also selectively move one of the two GFP-ParB/*par*S foci. Accordingly, we propose that GapR/OpaA displacement is a byproduct of its primary interactions with early partitioning motors. Replication is a likely candidate but we also propose that coupled transcription and translation have motive functions. In our Supplementary data (in Supplementary Figure S12), we present experiments that implicate both RNA polymerase and ribosomes. How GapR/OpaA might aid and guide the motors will be an important subject for future studies.

How is GapR involved in establishing chromosome asymmetry?

Bacterial chromosome replication and partition overlap temporally and this regulatory link is also implied by chromosome organization, because origins of replication often lie close to *par* loci. For example, in *C. crescentus Cori* and *parS* are separated by only 10 kb. These temporal and spatial linkages probably evolved to meet the special needs of bacteria and it should also be advantageous for both *par*S and *Cori* to share regulatory proteins. Interestingly, a recent

study also implicated the replication initiator DnaA during chromosome partitioning in *C. crescentus* (25). Therefore, replication and partitioning both utilize DnaA and GapR in *C. crescentus*. Similarly, in *Vibrio cholerae* and *Bacillus subtillis*, ParA interacts with DnaA to control replication (26,27).

Since chromosome replication precedes its partitioning, one might expect regulators to act sequentially, first at *Cori* and then at *parS*, but counter intuitively a recent study shows that as the activity of *C. crescentus* DnaA rises, it first acts at *parS* and then at *Cori*, because the threshold for DnaA action is lower at *parS* than at *Cori* (25). In a like manner, we see peak binding of GapR at *parB* immediately preceding the GapR binding interactions at *Cori* (*Cori* M and R) during the initiation of replication (Figure 3B). Therefore, while earlier cell cycle binding of GapR to *par*S at first appeared to be a paradox, it now agrees with an emerging view that both GapR and DnaA must respond to cell cycle signals and by as yet unknown mechanisms they must prepare *par*S in anticipation of replication initiation at *Cori*.

The early ParA-independent separation of *parS* loci is very important for asymmetric cell division, because this separation enables ParA, which moves from the distal pole, to bind just one chromosome for transport. Otherwise, if two ParB-*parS* loci are near when they encounter ParA, they risk being co-transported and not segregated (16,28,29). Therefore, while the ParA-system is 'blind' and chooses indiscriminately, it is the earlier GapR-utilizing system that 'sees' and discriminates between two alternative chromosomes. This is a key symmetry-splitting phase that channels the chromosomes into distinct *Sw*-pole versus *St*-pole programs (including alternative chromosome replication programs). Therefore, we propose that GapR facilities *C. crescentus* asymmetry. This role may also explain why GapR homologs are found exclusively in the α-proteobacteria (Supplementary Figure S13) (30) which typically divide asymmetrically and localize their origins of replication at the cell poles (31–33).

SUPPLEMENTARY DATA

Supplementary Data are available at NAR Online.

ACKNOWLEDGEMENTS

We also thank Drs S. Sagan, C. Maurice and T. Rolain for constructive criticisms of this manuscript.

FUNDING

Canadian Institutes for Health Research (CIHR) [operating grant MOP-12599 to G.T.M.]; Natural Sciences and Engineering Research Council of Canada (NSERC) [Rgpin 184894-09 to G.T.M.]; Swiss National Science Foundation (SNSF) [31003A_143660 to P.H.V.]. Funding for open access charge: CIHR.
Conflict of interest statement. None declared.

REFERENCES

1. Bartosik,A.A. and Jagura-Burdzy,G. (2005) Bacterial chromosome segregation. *Acta Biochim. Pol.*, **52**, 1–34.
2. Bastedo,D.P. and Marczynski,G.T. (2009) CtrA response regulator binding to the Caulobacter chromosome replication origin is required during nutrient and antibiotic stress as well as during cell cycle progression. *Mol. Microbiol.*, **72**, 139–154.
3. Wolanski,M., Donczew,R., Zawilak-Pawlik,A. and Zakrzewska-Czerwinska,J. (2014) oriC-encoded instructions for the initiation of bacterial chromosome replication. *Front. Microbiol.*, **5**, 735.
4. Marczynski,G.T., Rolain,T. and Taylor,J.A. (2015) Redefining bacterial origins of replication as centralized information processors. *Front. Microbiol.*, **6**, 610.
5. Laub,M.T., Shapiro,L. and McAdams,H.H. (2007) Systems biology of Caulobacter. *Annu. Rev. Genet.*, **41**, 429–441.
6. Mohl,D.A., Easter,J. Jr and Gober,J.W. (2001) The chromosome partitioning protein, ParB, is required for cytokinesis in Caulobacter crescentus. *Mol. Microbiol.*, **42**, 741–755.
7. Taylor,J.A., Ouimet,M.C., Wargachuk,R. and Marczynski,G.T. (2011) The Caulobacter crescentus chromosome replication origin evolved two classes of weak DnaA binding sites. *Mol. Microbiol.*, **82**, 312–326.
8. Quisel,J.D., Lin,D.C. and Grossman,A.D. (1999) Control of development by altered localization of a transcription factor in B. subtilis. *Mol. Cell*, **4**, 665–672.
9. Krzywinski,M., Schein,J., Birol,I., Connors,J., Gascoyne,R., Horsman,D., Jones,S.J. and Marra,M.A. (2009) Circos: an information aesthetic for comparative genomics. *Genome Res.*, **19**, 1639–1645.
10. Tsai,J.W. and Alley,M.R. (2001) Proteolysis of the Caulobacter McpA chemoreceptor is cell cycle regulated by a ClpX-dependent pathway. *J. Bacteriol.*, **183**, 5001–5007.
11. Christen,B., Abeliuk,E., Collier,J.M., Kalogeraki,V.S., Passarelli,B., Coller,J.A., Fero,M.J., McAdams,H.H. and Shapiro,L. (2011) The essential genome of a bacterium. *Mol. Syst. Biol.*, **7**, 528.
12. Bailey,T.L., Williams,N., Misleh,C. and Li,W.W. (2006) MEME: discovering and analyzing DNA and protein sequence motifs. *Nucleic Acids Res.*, **34**, W369–W373.
13. Fumeaux,C., Radhakrishnan,S.K., Ardissone,S., Theraulaz,L., Frandi,A., Martins,D., Nesper,J., Abel,S., Jenal,U. and Viollier,P.H. (2014) Cell cycle transition from S-phase to G1 in Caulobacter is mediated by ancestral virulence regulators. *Nat. Commun.*, **5**, 4081.
14. Marczynski,G.T., Lentine,K. and Shapiro,L. (1995) A developmentally regulated chromosomal origin of replication uses essential transcription elements. *Genes Dev.*, **9**, 1543–1557.
15. Thanbichler,M. and Shapiro,L. (2006) MipZ, a spatial regulator coordinating chromosome segregation with cell division in Caulobacter. *Cell*, **126**, 147–162.
16. Shebelut,C.W., Guberman,J.M., van Teeffelen,S., Yakhnina,A.A. and Gitai,Z. (2010) Caulobacter chromosome segregation is an ordered multistep process. *Proc. Natl. Acad. Sci. U.S.A.*, **107**, 14194–14198.
17. Ricci,D.P., Melfi,M.D., Lasker,K., Dill,D.L., McAdams,H.H. and Shapiro,L. (2016) Cell cycle progression in Caulobacter requires a nucleoid-associated protein with high AT sequence recognition. *Proc. Natl. Acad. Sci. U.S.A.*, **113**, E5952–E5961.
18. Arias-Cartin,R., Dobihal,G.S., Campos,M., Surovtsev,I.V., Parry,B. and Jacobs-Wagner,C. (2016) Replication fork passage drives asymmetric dynamics of a critical nucleoid-associated protein in Caulobacter. *EMBO J.*, **36**, 301–318.
19. Quon,K.C., Marczynski,G.T. and Shapiro,L. (1996) Cell cycle control by an essential bacterial two-component signal transduction protein. *Cell*, **84**, 83–93.
20. Domian,I.J., Quon,K.C. and Shapiro,L. (1997) Cell type-specific phosphorylation and proteolysis of a transcriptional regulator controls the G1-to-S transition in a bacterial cell cycle. *Cell*, **90**, 415–424.
21. Toro,E., Hong,S.H., McAdams,H.H. and Shapiro,L. (2008) Caulobacter requires a dedicated mechanism to initiate chromosome segregation. *Proc. Natl. Acad. Sci. U.S.A.*, **105**, 15435–15440.
22. Lemon,K.P. and Grossman,A.D. (2000) Movement of replicating DNA through a stationary replisome. *Mol. Cell*, **6**, 1321–1330.
23. Jun,S. and Mulder,B. (2006) Entropy-driven spatial organization of highly confined polymers: lessons for the bacterial chromosome. *Proc. Natl. Acad. Sci. U.S.A.*, **103**, 12388–12393.

24. Dworkin,J. and Losick,R. (2002) Does RNA polymerase help drive chromosome segregation in bacteria? *Proc. Natl. Acad. Sci. U.S.A.*, **99**, 14089–14094.
25. Mera,P.E., Kalogeraki,V.S. and Shapiro,L. (2014) Replication initiator DnaA binds at the Caulobacter centromere and enables chromosome segregation. *Proc. Natl. Acad. Sci. U.S.A.*, **111**, 16100–16105.
26. Kadoya,R., Baek,J.H., Sarker,A. and Chattoraj,D.K. (2011) Participation of chromosome segregation protein ParAI of Vibrio cholerae in chromosome replication. *J. Bacteriol.*, **193**, 1504–1514.
27. Murray,H. and Errington,J. (2008) Dynamic control of the DNA replication initiation protein DnaA by Soj/ParA. *Cell*, **135**, 74–84.
28. Hwang,L.C., Vecchiarelli,A.G., Han,Y.W., Mizuuchi,M., Harada,Y., Funnell,B.E. and Mizuuchi,K. (2013) ParA-mediated plasmid partition driven by protein pattern self-organization. *EMBO J.*, **32**, 1238–1249.
29. Ptacin,J.L., Gahlmann,A., Bowman,G.R., Perez,A.M., von Diezmann,A.R., Eckart,M.R., Moerner,W.E. and Shapiro,L. (2014) Bacterial scaffold directs pole-specific centromere segregation. *Proc. Natl. Acad. Sci. U.S.A.*, **111**, E2046–2055.
30. Gupta,R.S. and Mok,A. (2007) Phylogenomics and signature proteins for the alpha proteobacteria and its main groups. *BMC Microbiol.*, **7**, 106.
31. Jensen,R.B., Wang,S.C. and Shapiro,L. (2002) Dynamic localization of proteins and DNA during a bacterial cell cycle. *Nat. Rev. Mol. Cell Biol.*, **3**, 167–176.
32. Deghelt,M., Mullier,C., Sternon,J.F., Francis,N., Laloux,G., Dotreppe,D., Van der Henst,C., Jacobs-Wagner,C., Letesson,J.J. and De Bolle,X. (2014) G1-arrested newborn cells are the predominant infectious form of the pathogen Brucella abortus. *Nat. Commun.*, **5**, 4366.
33. Kahng,L.S. and Shapiro,L. (2003) Polar localization of replicon origins in the multipartite genomes of Agrobacterium tumefaciens and Sinorhizobium meliloti. *J. Bacteriol.*, **185**, 3384–3391.